

## Measurements of plasma-wave generation using a short-pulse high-intensity laser beat wave

B. Walton, Z. Najmudin, M. S. Wei, C. Marle, R. J. Kingham, K. Krushelnick,<sup>a)</sup> and A. E. Dangor

*Blackett Laboratory, Imperial College, London SW7 2BZ, United Kingdom*

R. J. Clarke, M. J. Poulter, C. Hernandez-Gomez, S. Hawkes, D. Neely, J. L. Collier, and C. N. Danson

*Central Laser Facility, Rutherford Appleton Laboratory, Chilton, Didcot, Oxon OX11 0QX, United Kingdom*

S. Fritzler and V. Malka

*Laboratoire d'Optique Appliquée, École Polytechnique, CNRS, 91761 Palaiseau, France*

(Received 8 September 2004; accepted 28 November 2005; published online 12 January 2006)

Experiments to examine the generation of relativistic plasma waves via a high-intensity short-pulse beat-wave scheme are described in detail. The pulse stretcher of the Vulcan chirped-pulse amplification (CPA) laser system was modified to produce two frequency, 3 ps pulses focusable to intensities up to  $10^{18}$  W cm<sup>-2</sup>. Short high-intensity pulses were used to avoid limitations to the plasma-wave amplitude due to the modulational instability. Two experiments were undertaken, at 3 and 10 TW, with the generation of plasma waves diagnosed by measuring the sidebands produced in the spectrum of the forward scattered beam. A resonance in the sideband signal was observed for an initial plasma density higher than expected for the given beat frequency. This resonance shift can be attributed to transverse ponderomotive expulsion of plasma electrons from the laser focal region. A monotonically increasing background was also observed, which was due to nonresonant cross-phase modulation. © 2006 American Institute of Physics. [DOI: 10.1063/1.2160517]

### I. INTRODUCTION

The plasma beat-wave acceleration (PBWA) scheme<sup>1</sup> is one of a number of methods of producing relativistic electron plasma waves via the interaction of an intense laser pulse with an underdense plasma. The PBWA scheme involves the copropagation through a plasma of two laser pulses of slightly differing frequencies,  $\omega_1$  and  $\omega_2$  (such that  $\omega_1 - \omega_2 = \omega_b \ll \omega_1, \omega_2$ ). The superposition of these laser fields creates a low-frequency beat pattern on the laser envelope with which there is an associated ponderomotive force. If the frequency of the force is resonant with the electron plasma frequency  $\omega_{pe}$ , a large-amplitude relativistic electron plasma wave (EPW) can be produced. These plasma waves are of particular interest, since they can be used to accelerate electrons efficiently to high energies in short distances.

Previous work has shown that the beat-wave scheme is a reliable and reproducible method for generating plasma waves having relativistic phase velocities.<sup>2-11</sup> The ultimate amplitude of the plasma waves produced is limited, however, by several factors—one of which is relativistic detuning. The growth of the wave proceeds only for as long as the beat frequency is closely tuned to the plasma frequency. As the wave amplitude grows, the plasma frequency decreases due to an increase of the electron mass via relativistic effects. This detunes the growth from resonance, placing an upper limit on the wave amplitude and preventing wave breaking and self-trapping of electrons. In addition, the EPW can decay via the modulational instability<sup>9,12,13</sup> over time scales on

the order of the ion plasma frequency  $\omega_{pi}$ . Hence it has long been realized that the time taken for the wave amplitude to reach the maximum possible amplitude (i.e., the relativistic limit) must be shorter than this.<sup>14</sup>

The (small amplitude) growth rate of the plasma waves generated by the PBWA is given by  $\dot{\epsilon} = \delta n/n_e = (1/4)a_1 a_2 \omega_{pe}$  (where  $a_i$  is the normalized vector potential of the  $i$ th component of the laser pulse). The plasma-wave amplitude saturates relativistically in a time  $\tau_{rel} = 4(\frac{16}{3})^{1/3}(a_1 a_2)^{-2/3}$  at  $\epsilon_{max} = (16a_1 a_2/3)^{1/3}$ .<sup>3</sup> Since  $a \propto (I\lambda^2)^{1/2}$ , many previous PBWA experiments have used long-wavelength laser systems such as CO<sub>2</sub> lasers,<sup>2-7</sup> where the beat wave is formed using simultaneous emission of two lasing lines near 10.6  $\mu$ m. Nd:glass lasers, which operate at  $\sim 1$   $\mu$ m, have also been used in beat-wave experiments.<sup>8-10</sup> In these experiments two separate beams are amplified in different amplifier chains with slightly different lasing frequencies [typically neodymium-doped yttrium aluminum garnet (Nd:YAG) and neodymium-doped yttrium lithium fluoride (Nd:YLF)]. Plasma waves produced by such higher-frequency driver have a greater phase velocity for a given plasma density, since the group velocity of the beat pattern driving its growth is higher—the Lorentz factor of the wave is given by  $\gamma_p \approx (\omega_0/\omega_{pe}) = (n_{cr}/n_0)^{1/2}$ , where  $n_{cr}$  is the critical density for a laser of frequency  $\omega_0$ . They can therefore potentially accelerate electrons to higher energies. However, the shorter wavelength of Nd:glass systems means that the growth rate for plasma waves is lower for equal intensities.

In this paper, a new configuration for beat-wave acceleration experiments is described in detail. This setup makes use of chirped-pulse amplification in the Vulcan Nd:glass

<sup>a)</sup>Electronic mail: kmkr@ic.ac.uk

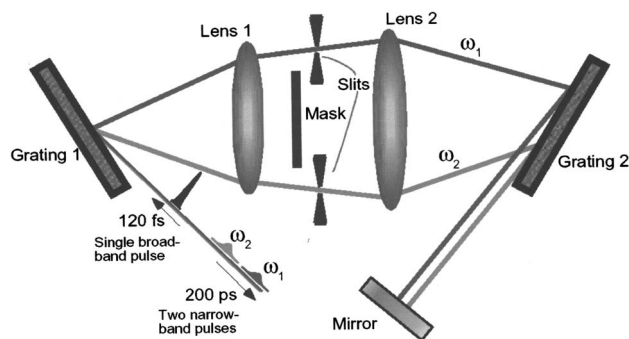


FIG. 1. (Color online) Modifications to the Vulcan CPA stretcher system for beat-wave production.

laser system in order to produce a shorter more-intense beat-wave driver than has been used previously,<sup>11</sup> thereby increasing the EPW growth rate and preventing saturation via the modulational instability.<sup>12</sup> The results of experiments using this system to generate relativistic plasma waves are described.

## II. ALTERATIONS TO THE VULCAN CPA SYSTEM FOR BEAT-WAVE EXPERIMENTS

The unmodified Vulcan chirped-pulse amplification (CPA) laser system is capable of producing laser pulses having a maximum energy of 100 J in 700 fs, corresponding to a beam power of approximately 140 TW. In order to produce the required dual frequency beam to generate a beat-wave modulation on the laser wave packet a mask is placed between the gratings of the CPA stretcher system.<sup>15</sup> The first stretcher grating disperses the laser spectrum in space, so by using a mask with two slits after this grating, two well-separated and relatively narrow bandwidths may be selected from the wider gain bandwidth of the laser. After emerging from the double pass stretcher the beam consists of two pulses propagating collinearly but separated in time (Fig. 1). This separation is advantageous as it prevents nonlinear mixing of the two pulses within the amplifiers further up the chain.

This modification of the CPA system introduces flexibility in the choice of wavelengths that can be used to produce the beat wave. To alter either of the transmitted wavelengths, the slits can be moved along the plane of dispersion. Additionally the bandwidth of each component can be altered by changing the corresponding slit width. This fine control of the spectrum is important as it is desirable to maximize the frequency difference between the two components (and hence to maximize the plasma-wave growth rate) while keeping the wavelength of each pulse inside the gain bandwidth of Nd:glass.

Placing a mask between the stretcher gratings reduces the bandwidth the laser system can amplify, with the consequence that the transform-limited pulse length is increased. Operating at the edges of the gain region in Nd:glass will also have the effect of reducing the efficiency of the amplifier chain—resulting in lower-energy pulses. This must be considered when selecting the width of each slit; if it is too

wide the contrast between the beat-wave minima and maxima may be low; too narrow and a low power pulse will result.

Similarly the bandwidth of the compressor must also be considered to optimize the throughput of the system. Since the two pulses are collinear, they overlap completely on the first compressor grating. Thereafter they are spectrally dispersed and their paths diverge, though there is still significant overlap at the second grating. Hence the two beams will walk off the center of the second compressor grating, which is ideally set for a central wavelength between the two beating wavelengths. This again limits the frequency difference between the two wavelengths. To maximize the laser energy while minimizing the effect of this walk off, the laser beams were asymmetric, typically  $20 \times 11$  cm, i.e., with an aspect ratio of approximately 2:1. This has obvious implications for the focusing of the beams.

Clearly, if sufficient resources are available, a three-grating compressor system may be employed, such that the two wavelengths diffract from the first grating onto two separate second gratings. Such a three-grating setup would have a particular advantage for beat-wave experiments since the power throughput could be greatly increased. In addition, a frequency “chirp” could be imposed on one or both of the pulses so that the beat frequency could be made to change over the length of the combined pulse. This would be desirable as it could potentially offset relativistic detuning of the plasma frequency with respect to the beat frequency at large wave amplitudes<sup>16</sup> (i.e., a corresponding “chirped” beat wave could be imposed on the wave packet). In order to do this most efficiently, the stretcher would also need to be modified as well.

## III. EFFECT OF THE INTERACTION ON THE LASER SPECTRUM

### A. Mixing of laser frequencies via plasma wave growth

The coupling of the plasma wave with the laser pulses can enable energy transfer from the initial laser frequencies  $\omega_{1,2}$  into spectral sidebands of frequency  $\omega_{1,2} \pm m\omega_b$ , where  $m$  is an integer and  $\omega_b$ , the beat frequency, is equal to  $\Delta\omega$ . This effect may be distinguished from nonlinear optical effects such as cross-phase modulation (XPM) by the resonant enhancement of the coupling when  $\omega_b = \omega_1 - \omega_2 \sim \omega_{pe}$ . Therefore as the plasma density is scanned, a peak should be observed superimposed upon any consistent increase in sideband amplitude due to nonresonant XPM. It should be stressed that such a spike in sideband intensity can only be produced through the coupling of the laser with a resonantly excited plasma wave, and so the height of the spike can be used to estimate the peak wave amplitude.

The plasma wave modifies the laser spectrum by causing the refractive index to vary periodically over time. For small wave amplitudes the expression for the refractive index of an inhomogeneous plasma contains a nonlinear correction  $\delta\eta(t)$ ,<sup>17</sup>

$$\eta(t) = \eta_0 - \frac{1}{2} \frac{n_e}{n_{\text{cr}}} \frac{\delta n(t)}{n_e}. \quad (1)$$

This density fluctuation couples the laser photons into sideband frequencies. In the limit of small  $\delta n_e$  and low sideband intensity,  $I_{\omega \pm \omega_b}$  and  $I_{\omega \pm 2\omega_b}$  can be expressed as<sup>18</sup>

$$\frac{I_{\omega \pm \omega_b}}{I_\omega} \approx \frac{1}{16} \left( \frac{\omega n_e}{c n_{\text{cr}} n_e} \frac{\delta \bar{n}}{L} \right)^2, \quad \frac{I_{\omega \pm 2\omega_b}}{I_{\omega \pm \omega_b}} \approx \frac{1}{16} \left( \frac{\omega n_e}{c n_{\text{cr}} n_e} \frac{\delta \bar{n}}{L} \right)^2, \quad (2)$$

where  $L$  is the propagation distance.

## B. Cross-phase modulation

In these experiments, the two beams travel partially overlapped from the compressor, onto the focusing off-axis parabolic mirror and then to focus. The recompressed pulses may be sufficiently intense along this path to generate sidebands due to atomic cross-phase modulation (AXPM). The nonlinear cross-correlated component contributes a component to the refractive index  $\eta$  proportional to  $\langle a_1 a_2 \rangle \eta_2$ . This term can thus mix frequencies  $\omega_{1,2}$  to generate a frequency  $\omega_b$ . The value of the nonlinear refractive index  $\eta_2$  is determined by the density and composition of the medium. It can be expressed in terms of the nonlinear hyperpolarizability  $\gamma = 4\epsilon_0 \eta_0 \eta_2 / 3n$ , where  $n$  is the gas molecular density. However, this expression is only accurate for small values of  $\eta_2$  with respect to  $\eta_0$ , since it is calculated via perturbation theory. Consequently at higher intensities ( $> 10^{15}$  W/cm<sup>2</sup>), numerical techniques must be employed to determine the hyperpolarizability, refractive index, and their dependence on incident laser intensity. The intensities of these sidebands (for small amplitude) can be calculated in the same way as for Eq. (2),<sup>19</sup>

$$\frac{I_{\omega \pm \omega_b}}{I_\omega} \approx \frac{9}{64} \left( \frac{n \gamma (\omega_1 \omega_2)^{3/2} m_e^2 c}{\epsilon_0 \eta_0 e^2} \langle a_1 a_2 \rangle L \right)^2, \quad (3)$$

where  $\gamma$  in this context is the nonlinear hyperpolarizability of the molecule. The energy in each sideband should therefore initially grow quadratically with gas density.

AXPM is enhanced when the frequency difference  $\omega_1 - \omega_2$  coincides with a transition between energy levels in the molecule. This resonant effect is particularly important at low laser intensities; however, at high enough intensity the nonresonant effect may be observed. As the H<sub>2</sub> molecule has no electric dipole moment, it interacts very weakly with far-infrared and microwave radiation: the frequency differences used during the experiments to be described here are  $1.15 \times 10^4$  and  $9.0 \times 10^3$  GHz, which do not correspond to any transition in hydrogen.

Relativistic cross-phase modulation (RXPM) can also occur in the plasma itself if the oscillation velocities of electrons in the laser field become relativistic, in which case the refractive index of an underdense plasma becomes

$$\eta(t) = \eta_0 + \frac{1}{4} \frac{n_e}{n_{\text{cr}}} \frac{\langle a_1 a_2 \rangle}{\langle a_1 a_2 \rangle + 1}, \quad (4)$$

where the time averaging is over the fast  $\omega_1 + \omega_2$  time scale. Using the derivation described in Ref. 18 the intensity of the first sideband produced through RXPM can be estimated to be

$$\frac{I_{\omega \pm \omega_b}}{I_\omega} \approx \frac{1}{16} \left( \frac{\omega n_e}{c n_{\text{cr}} \langle \bar{a}_1 \bar{a}_2 \rangle + 1} \langle \bar{a}_1 \bar{a}_2 \rangle L \right)^2, \quad (5)$$

where  $\langle \bar{a}_1 \bar{a}_2 \rangle$  indicates an average over the path length as well as over the fast frequency component. The sideband intensity should again grow quadratically with plasma density, at least for small values of  $I_{\omega \pm \omega_b}$ . However, at the intensities used in the experiments described here the effect of RXPM is likely to be much less than that due to atomic/molecular effects since the nonlinear polarizability of H<sub>2</sub> molecules is likely to become very important immediately before ionization, while relativistic plasma nonlinearities will not be significant until  $I > 1.5 \times 10^{18}$  W/cm<sup>2</sup>.

## IV. EXPERIMENTAL SETUP

Pulse compression in these experiments was achieved using a single-pass two-grating compressor system, and the beam was focused by an ( $f=45$  cm) off-axis parabolic mirror. In these experiments the gas targets used was hydrogen, as it is rapidly ionized by the leading edge of the laser pulse due to direct field ionization. To reproducibly produce an electron density of  $10^{16} - 10^{17}$  cm<sup>-3</sup> at focus, the target chamber was statically filled and the density was monitored with a pressure gauge. Therefore the beam propagated from the compressor gratings to focus in an atmosphere of low-density neutral gas can contribute to AXPM.

The beam transmitted through the plasma along the laser axis was recollimated by a spherical mirror and reflected out of the chamber. It was then focused by a similar mirror onto the slit of a 1 m optical spectrometer, where it was spectrally dispersed by a 600 line/mm grating. A 16 bit 256 × 1024 pixel charge-coupled device (CCD) camera was used as the detector.

Before the interaction, the beam is rectangular with dimensions 20 × 11 cm. This 2:1 asymmetry in aspect ratio results after focusing with the parabolic mirror in a minimum full width half maximum (FWHM) focal spot size of around 20–30 μm in one direction and a spot of about 10–20 μm in the other. This focusing geometry is not ideal for the production of high-quality collimated electron beams as the spot size is much smaller than the plasma wavelength at resonance, which is 170 μm. It is likely that the transverse ponderomotive forces acting at the beat frequency-produced plasma oscillations with a significant radial component—unsuitable for particle acceleration. Thus, these experiments were intended to be proof-of-principle investigations, designed primarily to produce and characterize plasma waves using this new CPA beat-wave setup rather than to drive the plasma waves to wave breaking and subsequently to generate directional high-energy electron beams.

We now try to quantify the effect of AXPM on the side-

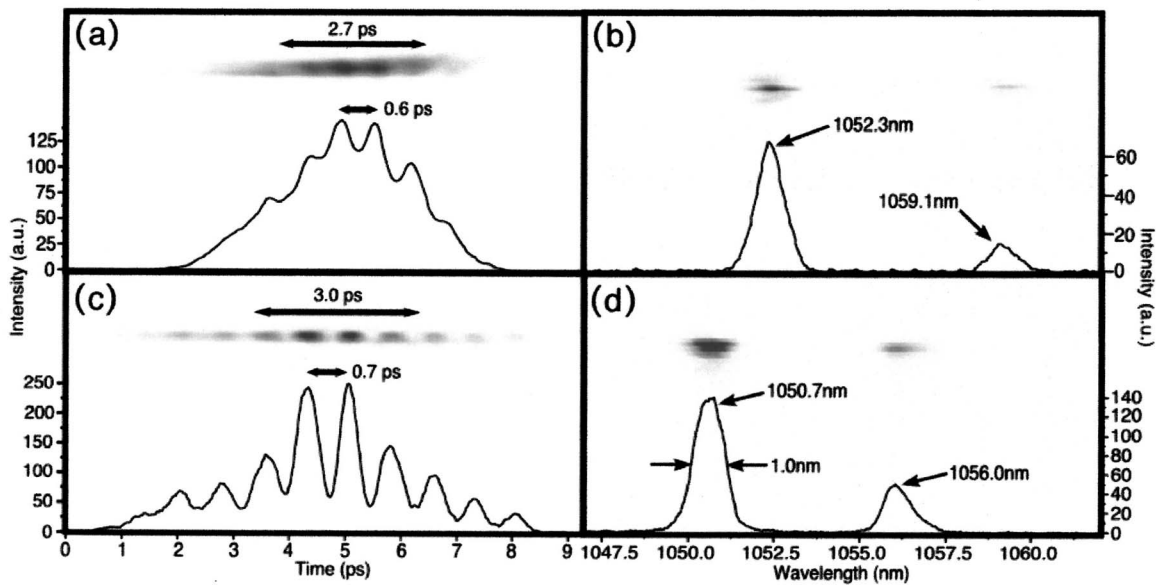


FIG. 2. (Color online) (a) Autocorrelation trace and (b) spectrum of the laser for the 3 TW experiment, and (c) autocorrelation trace and (d) spectrum of the laser for the 10 TW experiment. The spectra and the autocorrelation traces are not from the same shots.

band generation. After compression and *before* reaching the off-axis parabolic mirror, the collimated laser beam passes through from 0 to 30 mbar of low-pressure hydrogen gas. At the highest power (10 TW) the beams contained 30 J on average, 3:1 splitted between the two frequencies, in a  $20 \times 11$  cm beam. This gives a total intensity of  $4.5 \times 10^{10}$  W cm $^{-2}$  (assuming the frequency components are fully overlapped). The normalized field amplitudes of each component of the collimated beam are then  $a_1 = 1.8 \times 10^{-4}$  and  $a_2 = 7.9 \times 10^{-5}$ . The value of  $\gamma$  for the H $_2$  molecule at 1064 nm is  $\gamma = 43.37 \pm 0.10 \times 10^{-63}$  C $^4$  m $^4$  J $^{-3}$ , $^{20}$  so  $\eta_2$  at a molecular density of  $10^{17}$  cm $^{-3}$  will be  $3.67 \times 10^{-28}$  V $^{-2}$  m $^2$ . The AXPM correction to the refractive index by the collimated beam is then  $9.4 \times 10^{-11}$ , and the sidebands generated before the parabola will have an intensity [Eq. (3)]  $I_{\omega \pm \omega_b} / I_{\omega} \sim 1.2 \times 10^{-6}$ , which has a negligible effect on the laser spectrum.

The contribution of AXPM *after* the parabolic mirror as the laser converges towards focus can be estimated by integrating the laser intensity over the path between the mirror and the point where the intensity is large enough to ionize hydrogen through barrier suppression. The path integral of the intensity over a distance  $x$  after the mirror of focal length  $f$  is, using purely geometrical optics,  $\int_0^x I(x) dx = I(0) f^2 / (f - x_i)$ , where  $x_i$  is where the intensity reaches the ionization threshold ( $I_{\text{BSI}} = 1.4 \times 10^{14}$  W/cm $^2$ ). Expressing  $I$  in terms of  $\langle a_1 a_2 \rangle$ , a value  $I_{\omega \pm \omega_b} / I_{\omega} \sim 2.1 \times 10^{-5}$  is obtained. Though larger than the contribution before the parabolic mirror, this calculation by perturbation theory suggests that this component will also be insignificant. However, the value of  $\eta_2$  used here ( $3.79 \times 10^{-7}$  from the value of  $\gamma$  given above) will be greatly underestimated at intensities close to that required for ionization. Hence this estimate for sideband production is also likely to be greatly underestimated. Numerical calculation of these effects, taking into consideration the detailed atomic physics of the hydrogen atom, is necessary for a

proper estimate and are likely to give orders of magnitude increase in sideband intensity.

An estimate of the RXPM is expected to take place in the plasma, and this can be found by using the confocal length of the focusing optic as the path length ( $\sim 300$   $\mu$ m for an  $f/4$  focusing geometry with a nondiffraction limited beam) and the laser field amplitudes from the 10 TW experiment,  $a_1 = 1.4$  and  $a_2 = 0.8$ . Using these values, an estimate can be calculated using Eq. (5) of  $I_{\omega \pm \omega_b} / I_{\omega} \sim 8 \times 10^{-4}$ , for a density of  $n_e = 10^{17}$  cm $^{-3}$ . Since this value is small (and unlikely to be underestimated as was the case for AXPM), the sideband generation due to RXPM can be ignored.

## V. RESULTS FROM THE VULCAN EXPERIMENT AT 3 TW

Two experiments were undertaken with the Vulcan laser using the beat-wave setup. The laser was able to produce 2–3 TW for the first experiment and about 10 TW for the second.

In the first experiment, the laser produced an average of 8 J on target although a maximum of 14 J was obtained. A streak camera with picosecond temporal resolution was set up to monitor the prepulse, so that the relative energies in the prepulse and the main pulses could be seen. As shown in the spectrometer image and line out [Fig. 2(b)], the laser produces two wavelengths at  $\lambda_1 = 1052.3$  nm and  $\lambda_2 = 1059.1$  nm, which corresponds to a resonant electron density of  $4.15 \times 10^{16}$  cm $^{-3}$ . Each component had a bandwidth of 1.0 nm with the energy balance between the components being roughly 4:1 ( $\lambda_1 : \lambda_2$ ) on this shot. The autocorrelator trace indicates a pulse length of approximately 2.7 ps [Fig. 2(a)], and a beat pattern of period of 0.6 ps can be clearly discerned. This confirms that the two pulses were spatially and temporally overlapped at focus.

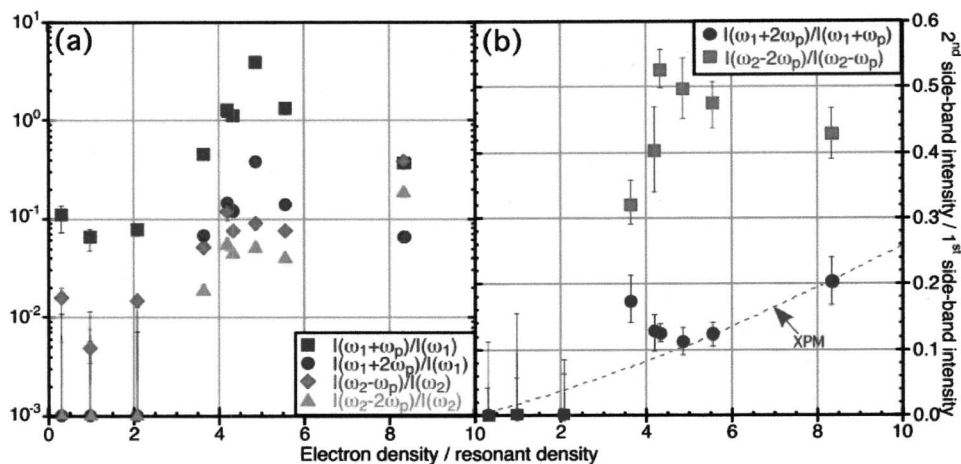


FIG. 3. (Color online) Variation of sideband intensities with electron density, for shots (with prepulse) into hydrogen. (a) shows the first and second red and blue sidebands normalized to the nearest fundamental, and (b) shows the ratio of the second to the first sideband. Error bars are determined from background level on detectors.

The FWHM focal spot size of  $30 \mu\text{m}$  gives an average on target intensity of about  $2.7 \times 10^{17} \text{ W cm}^{-2}$ . With an energy balance of 4:1, the pulses have field strengths of  $a_1=0.42$  and  $a_2=0.21$ . This gives a relativistic saturation time of  $\tau_{\text{rel}} \sim 3.1 \text{ ps}$ , so that at resonance  $\omega_{\text{pi}}\tau_{\text{rel}}=0.82$ . The plasma wave should therefore saturate relativistically rather than through the modulational instability. The relativistic wave amplitude limit with these parameters is  $\delta n/n_e=0.78$ .

In order to minimize the effects of AXPM, the beam was split into prepulse and main pulse by placing a block of glass inside the CPA stretcher after the mask. The block was positioned so that the entire beam at one frequency and part of the beam at the other frequency (the higher-energy component) had to travel through the glass. The light passing through the glass was delayed due to its higher refractive index than air; thus the component not passing through glass, becomes a single frequency prepulse. This prepulse will preionize the target, thus reducing the amount of AXPM at high intensity. A measurement with a streak camera showed that approximately 40% of the laser energy is in the prepulse. The energy in the beat wave is therefore reduced to an average of 4.7 J. This means that the average intensity was  $1.6 \times 10^{16} \text{ W cm}^{-2}$ , with an energy balance of 2.3:1,  $\tau_{\text{rel}}=3.7 \text{ ps}$ , and at resonant density  $\omega_{\text{pi}}\tau_{\text{rel}}=0.98$ .

After the interaction, the transmitted beam was directed onto the slit of the optical spectrometer. A 1064 nm notch filter was placed in front of the slit and tuned so that the fundamental frequencies were attenuated compared to the sidebands. The filter had a FWHM bandwidth of 8 nm, so that a clear signal from the sidebands was recorded while avoiding serious saturation of the camera with light from the (much brighter) unscattered part of the beam. Figure 3 is a plot showing the sideband intensity dependence upon density. The densities are scaled to the resonant density of the beat. In Fig. 3(a) the sideband intensity has been normalized to the energy in the fundamental nearest to that sideband.

The strength of each sideband follows an upward trend with plasma density (the result of XPM). There is a clear resonance at  $n_e \sim 5n_{e0}$  rising above this background upward trend (where  $n_{e0}$  is the resonant density), which is reproduced by all of the sidebands. This is indicative of the resonance between the beat wave and the plasma wave fre-

quency, although the fact that it occurs at such a high density was unexpected.

The ratios between first and second sidebands for both the low- (red) and high-frequency (blue) sides of the fundamental frequencies are shown in Fig. 3(b). It can be seen from this plot that for both sets of sidebands, the peak in these ratios occurs at slightly different density from each other, both at slightly lower density than the peak in Fig. 3(a). This is unexpected, as it was anticipated that both ratios would vary with the plasma wave amplitude. Also, the ratio on the red side is observed to be much larger than on the blue side.

These anomalies may be explained if the sidebands were themselves able to couple to the plasma wave so that radiation cascades from the first-order sidebands to the second order.<sup>21</sup> This process would be energetically more favorable on the red side than the blue, as it involves a reduction in photon energy rather than an increase (acting like “seeded” forward Raman scattering). An estimate of the plasma-wave amplitude using the blue sidebands would therefore be more accurate. Since the cascading effect will be more efficient at higher densities, this would shift the peak in the sideband ratio towards a higher density, which would explain the difference in position of the red and blue peaks.

By assuming that electromagnetic cascading is negligible for the blue sidebands, an estimate for the average amplitude of the plasma wave over the path length of the interaction can be made using Eq. (2). Before this can be done the effect of XPM must be estimated and subtracted from the sideband ratio. This involves fitting a curve, varying quadratically with density to the points around the resonance [dotted line in Fig. 3(b)] and subtracting it. The ratio at the peak of the resonance is then entered into Eq. (2) using an estimate of the path length. Since the beam is not diffraction limited the interaction length will be given due to the focusing geometry rather than the confocal parameter of the beam (which is equal to twice the Rayleigh range  $z_R = \pi\sigma_0^2/\lambda$ ). The focusing optic used in this experiment had an  $f/4$  geometry, giving  $L \sim 300 \mu\text{m}$ .

Subtracting the XPM-related component of the sideband ratios gives a peak ratio of approximately 0.1 at  $n_e \sim 3.5n_{e0}$ . From Eq. (2) this gives an average value of  $\varepsilon$  of about 2.

This is higher than the limit imposed by relativistic detuning, and so cannot be the result of coupling of the laser with the plasma wave directly into the second sideband. Rather it must be a secondary effect whereby the light in the first sideband (as well as other components of the spectrum) is scattered by the plasma wave into the second (i.e., electromagnetic cascading). This value of  $\varepsilon$  also shows that the assumption that  $\varepsilon \ll 1$ , which was used to derive Eq. (2), is not valid in these conditions.

## VI. RESULTS FROM THE VULCAN EXPERIMENT AT 10 TW

The low-energy output of the previous beat-wave experiment was attributed to the reduced bandwidth for amplification due to the mask in the CPA stretcher. This resulted in the energy in the beam reaching subsequent amplifiers being below saturation level, and so the amount of energy extracted from each amplifier was drastically reduced. The dramatic shot-to-shot energy variations in that experiment were also due to this. The lack of fluence was remedied by mounting an additional 9 mm diameter preamplifier after the stretcher.

The result was an output up to 45 J on target. With a 30  $\mu\text{m}$  diameter focal spot and a 30 J pulse, and the intensity at focus is  $1.3 \times 10^{18} \text{ W cm}^{-2}$ . The pulse length ( $\sim 3$  ps) and the beat modulations are clearly depicted in the autocorrelator image shown in Fig. 2(c). The two beat-wave wavelengths were  $\lambda_1 = 1050.7 \text{ nm}$  and  $\lambda_2 = 1056.0 \text{ nm}$  [as shown in Fig. 2(d)], giving a beat period of about 700 fs and a resonant density of  $7.78 \times 10^{16} \text{ cm}^{-3}$ . The average energy balance was about 3:1 ( $\lambda_1 : \lambda_2$ ) which gives  $a_1 = 1.4$  and  $a_2 = 0.8$ . With these parameters  $\tau_{\text{rel}} = 1.2 \text{ ps}$  and  $\omega_{\text{pi}} \tau_{\text{rel}} = 0.25$  at resonance. So once again saturation occurs through relativistic effects rather than the modulational instability.

A static fill of hydrogen gas was again used as the target for this experiment. Shots were taken over a range of gas densities, and the spectrum of the beam transmitted through the plasma was recorded on a CCD camera. In this experiment, however, no notch filter was used in front of the slit of the spectrometer since stronger sidebands were produced, lessening the need for selective filtering of the two fundamentals. For the same reason, no prepulse was used in this experiment.

A plot of sideband intensities, scaled to the closest fundamental frequency, against electron density is shown in Fig. 4. In this density scan, the laser energy was reproducible to within 10%, and no preselection of data was required. A resonance at  $\sim 12n_{e0}$  can be clearly seen, again a signature of plasma wave production. The difference in the densities at which resonance occurs from the 3 to 10 TW experiment implies that there is an intensity dependence to the effective plasma density. The peak in sideband intensity corresponding to the resonance sits upon a slope rising linearly with density, again due to AXPM. It is also possible that there is a much smaller resonance at a lower density, at  $n_e \sim n_{e0}$ , it seems from this that the beat wave is resonant at two very different frequencies. The results from the first experiment also suggested a second small peak at  $n_e \sim n_{e0}$ , although this was not very clear.

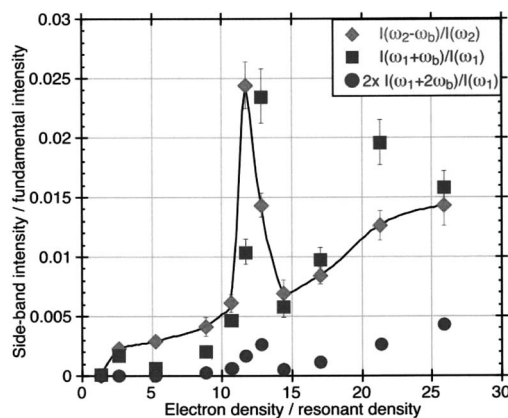


FIG. 4. (Color online) Plot of sideband intensities against plasma electron density with a 10 TW beat-wave pulse. A line has been traced through the points showing the first red sideband intensity to highlight the resonance at  $n_e \sim 12n_{e0}$ .

The stronger cascading effect in the longer wavelength sidebands is demonstrated by the linear increase of the background (AXPM) intensity with density to longer wavelength. This suggests that the cascading process is saturating. Both the first and the second sidebands to shorter wavelength increase quadratically with density, suggesting that the cascading to these sidebands is not yet saturated. As the fundamental at  $\omega_2$  was much lower in amplitude than that at  $\omega_1$ , the second (red) sideband to longer wavelength was not visible.

Equation (2) may be used to estimate the plasma-wave amplitude achieved during the experiment, assuming that sideband cascading can be ignored and the plasma-wave amplitude remains small. Hence once more using the blue sidebands and taking  $L = 300 \mu\text{m}$ , one obtains  $\delta\bar{n}/n_e \sim 0.1$ .

## VII. DISCUSSION

A mechanism that causes a shift in the resonance must be able to reduce the effective plasma frequency that the laser encounters during the interaction, so that the beat wave encounters resonant plasma even though the ambient electron density is nonresonant. As the shift appears to increase with intensity, so must the effect of the mechanism. Two processes that are possible sources of the observed change in the resonance condition are discussed here: relativistic electron mass increase and transverse ponderomotive expulsion of electrons.

The mass of an electron will increase as its oscillation velocity in the laser field approaches light speed. This is a separate process to relativistic detuning of the beat wave, which involves oscillations in the EPW. The mass increases with the relativistic factor, which in a linearly polarized laser field of amplitude  $a$  is equal to  $\gamma = (1 + a^2/2)^{1/2}$ . As the electron inertia climbs the plasma frequency drops, as  $\omega_{\text{pe}} \propto \gamma^{1/2}$ . To achieve resonance a higher electron density is required to compensate for the relativistic electrons and so the resonant density increases. A beat-wave pulse with 30 J will have a peak  $a = 1.6$ , so that  $\gamma = 1.5$ , and so the resonant density will also increase by a factor of 1.5. This is small compared to our observed shift and thus cannot account for the effect.

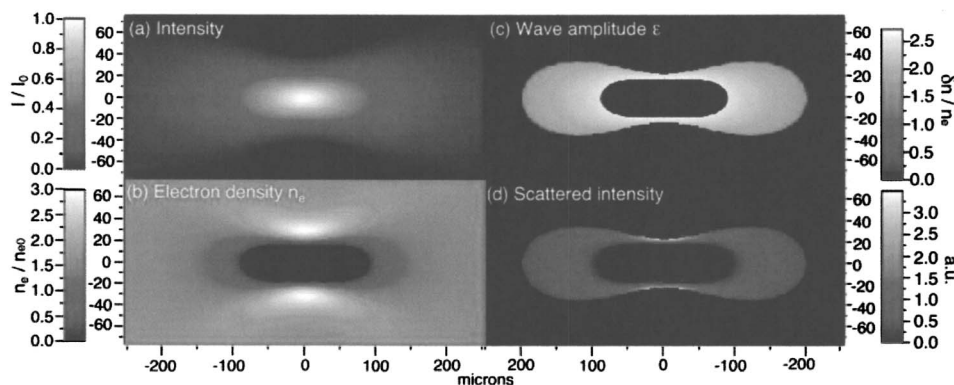


FIG. 5. (Color online) The calculation of the sideband intensity using 2D grids for a 3 ps, 30 J pulse with a 30  $\mu\text{m}$  spot size. (a) The distribution of average intensity over time is calculated using Eq. (7). (b) The modified electron-density distribution is found using Eq. (6). (c) The wave amplitude limited by the allowed density mismatch and the relativistic saturation mechanism is assigned to each point. (d) An estimated “strength of scattering” is calculated.

As was stated previously, the laser spot size is much smaller than the beat wavelength so that the magnitude of the transverse component of the ponderomotive force is somewhat larger than the longitudinal component. This has the effect of pushing electrons away from the peak of the laser pulse and lowering the density on axis. A region of positive charge is produced which in turn inhibits further electron-density depletion. An estimate of the extent of this depletion can be made by considering a steady-state situation where the magnitude of the ponderomotive force is constant, and then calculating the space-charge field that would exactly counter it.<sup>22</sup> An intensity profile of the form  $I(r, t) = I_0 e^{-2r^2/\sigma_0^2} e^{-2t^2/\tau^2}$ , where  $I_0$  is the intensity at the peak of the pulse,  $\sigma_0$  is the focal spot size, and  $\tau$  is the pulse duration, will exert a radial ponderomotive force  $F_p = -(e^2/4\epsilon_0 m_e \omega_1 \omega_2) \partial I / \partial r$ . Equating this to the space-charge force modifies the density by  $\delta n(r)$ . Expressed in terms of the total laser energy  $W$  in both pulses of the beat wave this is

$$\delta n(r) = \frac{4\sqrt{2}W}{\pi^{3/2} m_e c \omega_1 \omega_2 \sigma_0^4 \tau} \left(1 - \frac{2r^2}{\sigma_0^2}\right) \exp\left(-\frac{2r^2}{\sigma_0^2}\right). \quad (6)$$

If the laser propagates through a plasma with an initial density greater than the resonant value, the beam can reduce the density on axis so that it is resonant with the beat there. Indeed for a wide range of densities the effect of ponderomotive expulsion will be to produce some region having a resonant density in which plasma waves can be produced.

Although the transverse ponderomotive mechanism seems to be sufficient to cause the shift in the resonant density that is necessary for this effect to be observed, it is interesting to investigate how transverse effects interact with the other aspects of the beat-wave process, such as growth rate and saturation, to produce the variation in sideband amplitudes observed experimentally.

We can illustrate the effects of ponderomotive expulsion of electrons using a simple numerical calculation. First, the intensity distribution of the beam in the space immediately surrounding the focus is inscribed upon a two-dimensional (2D) array, so that every point on the array contains the laser intensity due to both pulses (averaged over the pulse length) that pass through that position. Such a distribution could be, for a Gaussian beam with energy  $W$ ,

$$\langle I(r, z) \rangle = \frac{W}{\pi \sigma^2(z)} \exp\left(-\frac{2r^2}{\sigma^2(z)}\right), \quad \sigma(z) = \sigma_0 \left(1 + \frac{z^2}{z_R^2}\right)^{1/2}, \quad (7)$$

where  $\langle I \rangle$  denotes an average over the pulse length  $\tau$ . An electron-density distribution can be defined in a similar array by choosing an ambient density and then using Eq. (6), again letting  $\sigma$  vary over  $z$ , to find the degree of electron cavitation or displacement imposed on the plasma by the transverse ponderomotive force of the laser. The laser intensity and electron density at identical points on both grids are compared, and a new array that contains the final wave amplitude at every point is generated using the equations for plasma-wave growth rate along with the expressions for linear and nonlinear detuning amplitudes. The linear detuning accounts for the mismatch between the electron density and the resonant density, so that  $\epsilon_{\text{max}} = a_1 a_2 [\omega_p / 2(\omega_p - \omega_b)]$ .

It now remains to obtain an estimate of the sideband intensities that might be produced for these experimental parameters. According to Eq. (2), the relative sideband intensity is proportional to  $(n_e \epsilon L)^2$ , where  $\epsilon$  is the wave amplitude and  $L$  is the path length of the beam through the wave. However, as this is not a ray-tracing program, it is difficult to gain a value for  $L$  for each part of the beam. To get around this, a new grid is constructed containing the values of  $I(n_e \epsilon)^2$ , and all the values in this new grid is summed to give a rough indication of the strength of the scattering of the laser by the wave. The inclusion of the intensity factor in this calculation has the effect of weighting the scattering in favor of regions close to focus. This is because the laser fluence through regions away from focus is smaller than at focus, so there is less laser energy per unit volume in those regions to couple to the plasma compared to the focal region. Figure 5 illustrates the steps of the calculation, and Fig. 6 shows the results. A similar methodology has previously been implemented,<sup>4</sup> although in that case phase information was retained to get a more accurate measure of the accumulated scattered intensity. However, our simple model will suffice for illustration.

Figure 6 shows that as the laser intensity increases (through an increase in pulse energy or a decrease in spot size), the density range broadens to become a plateau bordered by two sharp cutoffs. At the low-density end of the

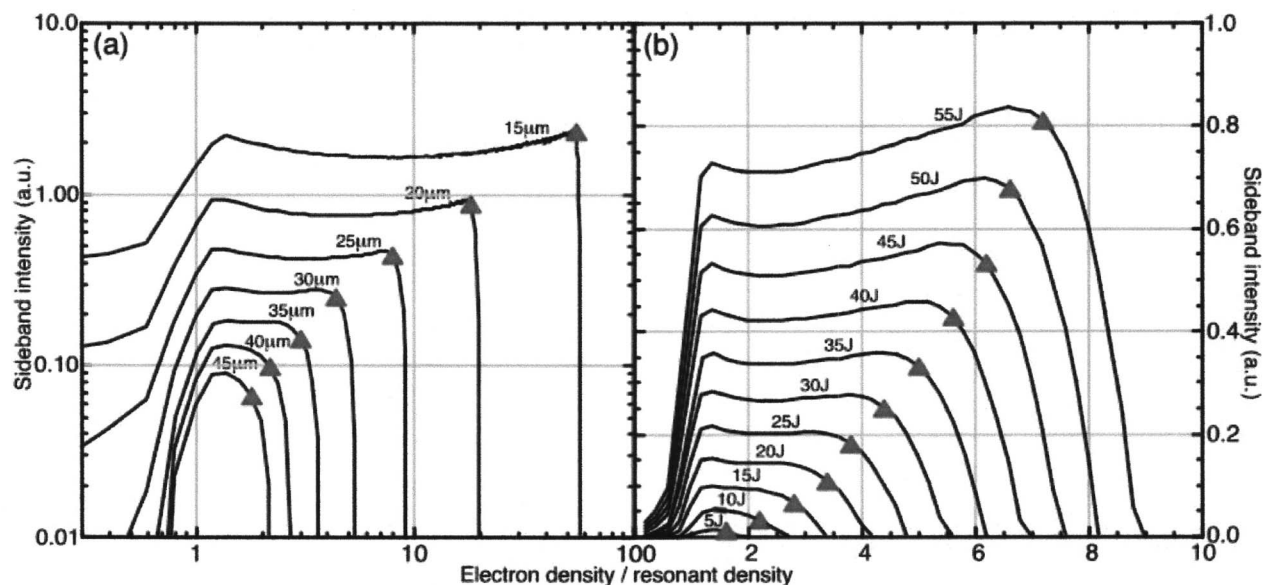


FIG. 6. (Color online) A plot of the variation of estimated “sideband intensity” with ambient electron density for a 3 ps duration pulse with 30  $\mu\text{m}$  focal spot, and with (a) pulse energy ranging from 5–55 J and (b) focal spot size  $\sigma_0$  ranging from 10–45  $\mu\text{m}$ . The triangles represent the ambient electron density above which the minimum density in the interaction is greater than the resonant density.

plateau, most of the plasma-wave production takes place away from focus, as the ponderomotive effect decreases as  $\sigma_0^{-4}$  whereas the wave growth rate falls as  $\sigma_0^{-2}$ . This means that, although the laser is intense enough to grow a large plasma wave, significant cavitation does not take place. Therefore scattering occurs over a large region, but at relatively low laser intensity. At the other end of the plateau, strong cavitation at focus brings the density there down to the resonant value so that plasma waves can be resonantly excited. Although this only occurs in a small region, the laser intensity is at its highest and the scattering is strong there. The cutoffs occur when there is no point in the plasma at resonance, either because the ambient density is too low or the effect of cavitation is too weak. As the strength of the cavitation increases as  $\sigma_0^{-4}$ , the position of the high-end cutoffs is extremely sensitive to focal spot size.

As noted above, these calculations cannot be used as a direct comparison with experiment since the wave amplitude given in Fig. 5(c) is actually a complex amplitude with magnitude and phase. The phase, even if calculated on a simple 2D grid, is an integral over time and changes with density and time very rapidly near resonance implying that it is difficult to obtain an estimate of the scattered amplitude into the sidebands from such considerations. In addition because the focal spot conditions were asymmetric and nondiffraction limited this means it would be necessary to do a three-dimensional (3D) calculation with an accurate focusing geometry—in order to compare directly to experiment.

Furthermore, the calculation does not take account of the finite spatial extent of the regions in which the wave is calculated to be resonantly excited, which could significantly affect the way that electrons oscillate in those regions. For example, in the middle of the two cutoff points of plateau in Fig. 6, most of the scattered light comes from a ring around the focus which is much narrower than the spot size or the

plasma wavelength. The electrons in this “ring” would not feel the same electrostatic return force as in a plane wave, so the frequency of oscillations would be greatly altered, and so scattering from this region can be ignored. If this source of scattering were to be discounted, there would remain two peaks in sideband growth, one next to the low-density cutoff and the other next to the cutoff at high density. This would be in agreement with the result of the density scan performed in both experiments, although the large-amplitude difference between those two peaks is not reflected here.

Nevertheless, these calculations clearly indicate that the effect of ponderomotive cavitation can produce the observed changes in resonant density. We have recently become aware of work where sidebands were observed in a beat-wave experiment that also had  $\omega_b \gg \omega_p$ .<sup>23</sup> These were described as coming from forced off-resonance radial plasma waves, which could scatter a probe beam in the forward direction. We should note that this mechanism might also contribute to our observed upward trend of the sideband light below the clear resonance peak (in addition to AXPM).

## VIII. CONCLUSIONS

The characteristics of the transmitted optical spectra, which were measured during these experiments, have shown that large-amplitude plasma waves have been created by the beat-wave interaction. When a scan in target plasma density was carried out, both with a 3 and 10 TW beat waves, peaks in the intensities of scattered sidebands in the transmitted spectra were observed. These were the results of resonances, which are due to an interaction between the two laser frequencies and an electron plasma wave. These resonances were displaced from the density for  $\omega_{pe} = \omega_2 - \omega_1$ , and the only mechanism that could cause this displacement is the transverse ponderomotive force of the narrow laser pulse

forcing electrons out of the beam and bringing the electron density in a large region of the interaction close to the resonant value. To illustrate this effect a simple calculation of the effect of ponderomotive charge displacement was constructed and it was found to be able to show how the experimentally observed resonance shift could occur.

As well as the resonance resulting from the mixing between the laser frequencies and the plasma wave, there was a monotonic increase with plasma density in spectral sideband intensities, indicating the occurrence of cross-phase modulation (XPM). This is believed to be caused by the nonlinear refractive indices of the hydrogen gas traversed before focus. There were also indications that a secondary scattering process took place whereby light cascaded between the spectral sidebands, not only between the fundamental laser frequencies and the sidebands.

Although large-amplitude plasma waves were created during these experiments, these waves would have been far from planar, as the focal spot size was much smaller than the plasma wavelength. Such an interaction would be very inefficient in accelerating electrons to high energies in a well-collimated beam. It is thought that future experiments, using a focusing optic with a larger  $f$  number or a phase-zone plate in order to increase the size of the focal spot relative to the plasma wavelength, will result in more planar plasma waves. Increasing the spot size means lowering the laser intensity, so a more powerful laser than used here would be required to reach comparable plasma-wave amplitude.

<sup>1</sup>T. Tajima and J. M. Dawson, Phys. Rev. Lett. **43**, 267 (1979).

<sup>2</sup>C. E. Clayton, C. Joshi, C. Darrow, and D. Umstadter, Phys. Rev. Lett. **54**, 2343 (1993).

<sup>3</sup>C. E. Clayton, K. A. Marsh, A. Dyson, M. Everett, A. Lal, W. P. Leemans, R. Williams, and C. Joshi, Phys. Rev. Lett. **70**, 37 (1993).

<sup>4</sup>C. E. Clayton, M. J. Everett, A. Lal, D. Gordon, K. A. Marsh, and C. Joshi, Phys. Plasmas **1**, 1753 (1994).

<sup>5</sup>Y. Kitagawa, T. Matsumoto, T. Minamihata, K. Sawai, K. Matsuo, K.

Mima, K. Nishihara, H. Azechi, K. A. Tanaka, H. Takabe, and S. Nakai, Phys. Rev. Lett. **68**, 48 (1992).

<sup>6</sup>N. A. Ebrahim, J. Appl. Phys. **76**, 7645 (1994).

<sup>7</sup>S. Y. Tochitsky, R. Narang, C. V. Filip, P. Musumeci, C. E. Clayton, R. B. Yoder, K. A. Marsh, J. B. Rosenzweig, C. Pellegrini, and C. Joshi, Phys. Plasmas **11**, 2875 (2004); S. Y. Tochitsky, R. Narang, C. V. Filip, P. Musumeci, C. E. Clayton, R. B. Yoder, K. A. Marsh, J. B. Rosenzweig, C. Pellegrini, and C. Joshi, Phys. Rev. Lett. **92**, 095004 (2004).

<sup>8</sup>A. E. Dangor, A. K. L. Dymoke-Bradshaw, and A. E. Dyson, Phys. Scr., T **T30**, 107 (1990).

<sup>9</sup>F. Amiranoff, M. Laberge, J. R. Marques, F. Moulin, E. Fabre, B. Cros, G. Matthieussent, P. Benkheiri, F. Jacquet, J. Meyere, P. Mine, C. Stenz, and P. Mora, Phys. Rev. Lett. **68**, 3710 (1992).

<sup>10</sup>F. Amiranoff, D. Bernard, B. Cros, F. Jacquet, G. Matthieussent, P. Mine, P. Mora, J. Morillo, F. Moulin, A. E. Specka, and C. Stenz, Phys. Rev. Lett. **74**, 5220 (1995).

<sup>11</sup>B. Walton, Z. Najmudin, M. S. Wei, C. Marle, R. J. Kingham, K. Krushelnick, A. E. Dangor, R. J. Clarke, M. J. Poulter, C. Hernandez-Gomez, S. Hawkes, D. Neely, J. L. Collier, and C. N. Danson, Opt. Lett. **27**, 2203 (2002).

<sup>12</sup>M. N. Rosenbluth and C. S. Liu, Phys. Rev. Lett. **29**, 701 (1972).

<sup>13</sup>P. Mora, D. Pesme, A. Heron, G. Laval, and N. Silvestre, Phys. Rev. Lett. **61**, 1611 (1988).

<sup>14</sup>C. Joshi, C. E. Clayton, W. B. Mori, J. M. Dawson, and T. Katsouleas, Comments Plasma Phys. Controlled Fusion **16**, 65 (1994).

<sup>15</sup>D. Neely, J. L. Collier, R. Allott, C. N. Danson, S. Hawkes, Z. Najmudin, R. J. Kingham, K. Krushelnick, and A. E. Dangor, IEEE Trans. Plasma Sci. **28**, 1116 (2000).

<sup>16</sup>A. Ghizzo, P. Bertrand, J. Lebas, T. W. Johnston, and M. Shoucri, Phys. Plasmas **5**, 4041 (1998).

<sup>17</sup>W. B. Mori, IEEE J. Quantum Electron. **33**, 1942 (1997).

<sup>18</sup>A. K. Lal, D. Gordon, K. Wharton, C. E. Clayton, K. A. Marsh, W. B. Mori, C. Joshi, M. J. Everett, and T. W. Johnston, Phys. Plasmas **4**, 1434 (1997).

<sup>19</sup>G. P. Agrawal, *Nonlinear Fiber Optics* (Academic, San Diego, 1995).

<sup>20</sup>D. P. Shelton, Phys. Rev. A **42**, 2578 (1990).

<sup>21</sup>B. I. Cohen, A. N. Kaufman, and K. M. Watson, Phys. Rev. Lett. **29**, 581 (1972).

<sup>22</sup>A. Dyson, A. E. Dangor, A. K. L. Dymoke-Bradshaw, T. Ashfar-Rad, P. Gibbon, A. R. Bell, C. N. Danson, C. B. Edwards, F. Amiranoff, G. Matthieussent, S. J. Karttunen, and R. R. E. Salomaa, Plasma Phys. Controlled Fusion **38**, 505 (1996).

<sup>23</sup>C. V. Filip, R. Narang, S. Ya. Tochitsky, C. E. Clayton, P. Musumeci, R. B. Yoder, K. A. Marsh, J. B. Rosenzweig, C. Pellegrini, and C. Joshi, Phys. Rev. E **69**, 026404 (2004).